Shahrood University of Technology

Journal of Mining and Environment (JME)

Journal homepage: www.jme.shahroodut.ac.ir

Iranian Society of Mining Engineering (IRSME)

A Deep Neural Network for Classification of Land Use Satellite Datasets in Mining Environments

Ajay Kumar[1], Yadvendra Pratap Singh[1], Aditya Gupta [1*], and Monu Bhagat[1]

School of Computer Science and Information Technology, Manipal University Jaipur, Jaipur, Rajasthan, India

Article Info

Received 8 September 2022

Received in Revised form 8 September 2022

Accepted 27 September 2022

Published online 27 September 2022

DOI:10.22044/jme.2022.12262.2224

Keywords

Satellite image

Dataset

Mining region

Land use

Deep neural network

Abstract

Land use (LU) is one of the most imperative pieces of cartographic information used for monitoring the mining environment. The extraction of land use data sets from remotely sensed satellite images has garnered significant interest in the mining region community. However, classification of LUs from satellite images remains a tedious task due to the lack of availability of efficient coal mining related datasets. Deep learning methods provide great leverage to extract meaningful information from high-resolution satellite images. Moreover, the performance of a deep learning classification approach significantly depends on the quality of the datasets. The present work attempts to demonstrate the generation of satellite-based datasets for the performance analysis of different deep neural network (DNN)-based learning algorithms in the LU classifications of mining regions. The mining regions are broadly classified into distinct regions based on visual inspection, namely barren land, built-up areas, waterbody, vegetation, and active coal mines. In our experimental work, a patch of 100 spatial samples for each of the five features is generated on three scales, as [1 × 1 × 3], [5 × 5 × 3], and [10 × 10 × 3]. Moreover, the effects of different scalabilities of the dataset on classification performances are also analyzed. Furthermore, this case study is implemented for the large-scale benchmark of satellite image datasets for mining regions. In the future, this work can be used to classify LU in the relevant study regions in real time.

1. Introduction

Mining land information contemplates socio-demographic facts, and is considered indispensable for planning and administration [26]. It also provides important input into areas of mining activity, critical for understanding the complex relationships between coal mining areas and other locations [10]. With the expansion of innovative remote sensing technologies, an enormous number of open-source satellite images are widely used, providing new possibilities for mining LU information [17]. However, the spatial features of mining terrain observed using satellite imagery are extremely complex and multi-faceted, conflating various other surfaces (built-up areas, barren areas, etc.). Due to the diversity and complexity of spatial features, classifying mined regions into different LU classes is an extremely challenging task. Therefore, a reliable and robust mining LU classification method must be developed by accurately delineating the spatial patterns or structures in satellite perception data.

In recent years, a lot of work has been done on developing advanced artificial intelligence-based LU classification methods. A satellite image comprises a set of pixels with similar spectral or morphological properties to each individual class [22], although, the number of pixel-based and object-based classification approaches exist in general. Predominantly, pixel-based approaches are utilized to perform mining region classifications. In a pixel-based approach, the spectral information related to each pixel is used as each feature type contains paramount semantic information [19]. Typically, feature classes used for classification include patterns of geometry, size, color, surface, shadow, location, and

✉ *Corresponding author: aditya.gupta@jaipur.manipal.edu (A. Gupta).*

association [1]. At the current time, many satellite sensors capture high spatial resolution data. Thus, these high-resolution data have significant potential for research in mining, including LU studies. However, the challenging task is the unavailability of coal mines related datasets for the classification algorithm. Many researchers have designed diverse types of datasets from other sources of images like aerial images, terrestrial images, microscopic images, and satellite images for examining the performances of different classification algorithms. The spatial resolution represents the quality of visualization of satellite images in the level of pixel-like high, medium, and low [25]. Also, it is a holistic representation of pixels but the many aspects of artificial neural network (ANN) learning techniques. It is fitted for large-scale data interpretation, examination, and pattern classification. Satellite images of spatial resolution directly affect a learning pattern to a performance matching. Also, it boosts supervised, unsupervised, semi-supervised, and reinforcement models [21] [24]. A quality dataset is the backbone of a machine learning algorithm for facilitating good training to model. The current work focuses on the generation of satellite-based datasets for comparative performance analysis of various classification algorithms.

In the past, many standard data sets were designed and used in the ANN and convolutional neural network (CNN) learning algorithms. The performance of a few of these algorithms is summarized in Table 1. A dataset, LCZ (Local Climate Zone), was standardized using sentinel-2B satellite data to classify the local climate zone (LCZ) in Mumbai [23]. The UC Merced dataset of spatial resolution (0.3 m) and pixels (256 × 256) size was generated using the airborne sensor for land-use classification [4]. A dataset, Indiana Pines, of spatial resolution (20 m) was prepared by the Purdue University using an airborne sensor to classify Pines in agricultural land in Tippecanoe, Indiana, USA [13]. An image dataset, GEOBIA, was designed by the University of California, Irvine (IUC) for image classification into nine classes [7]. A dataset, BCS, was designed by the State of Minas Gerais, Brazil using images captured in SPOT sensor for classifications into coffee and non-coffee region [11].

Table 1. Standardized image dataset used in image classification using ANN/CNN models.

Sl. No.	Dataset	Class	Total samples	Model	Accuracy (%)
1	LCZ	14	3500	ANN	72
2	UC Merced	21	2100	CNN	88.4 to 98
3	Indiana Pines	8	9144	ANN	85.1
4	GEOBIA	8	675	ANN	67.5
5	BCS	2	50000	CNN	82.6 to 99.3

1.1. Motivation and objective

Even though there are lot of research opined on using pixel-based, a hybrid of these two, for finding a subset of the most informative land-use features for better finding, still there is a lot to achieve in terms of performance with new feature selection methods for obtaining new insights into the land-use regions. Considering mining region selection is a non-deterministic polynomial time (NP)- hard problem and finding optimal mining surface from mining expression profiles is really a challenge for getting predictive accuracy. There are several offers for using the classification and clustering approaches to address the problem. Still, the land-use dataset provides a novel multi-objective optimization, and is a suitable classifier for addressing the Binary or Multi-class. Thus, efficient sample scale sizes of the LU dataset are chosen using model optimization, including a particular twelve classifiers training algorithm (Shown in Figure 1.). Further, we have compared twelve classifiers of training algorithms to check the effectiveness model. Thus, it motivated us to carry out further experiments using the DNN (Deep Neural Network) algorithm to assess the effect of land use classification of mining regions using different sample sizes of land use datasets for improved performance in diverse mining region datasets with five class classifications.

1.2. Article outline

The rest of the article is outlined as follows. Section 2 explains the materials and methods followed to conduct the study. In section 3, a description of different datasets is provided. Section 4 discusses the results. Finally, Section 5 concludes the work.

2. Materials and methods

The adopted methodology is shown in Figure 1, as followed by the steps of different sections of the working block to study the altered sample sizes of the different LU datasets.

2.1. Acquisition of satellite images and pre-processing of data

The present work used scenes captured by the Sentinel satellite sensor. Though the sentinel sensor offers 13- spectral bands, the current study only used data from three bands (B4, B3, and B2). The characteristics of the data are summarized in Table 2. The raw data of satellite images are pre-processed for designing the benchmark dataset. A false-color composite (FCC) image was prepared using the R, G, and B band data. Subsequently, the LU classes were extracted from the FCC image for spatial feature visualization with the known location in the google earth image.

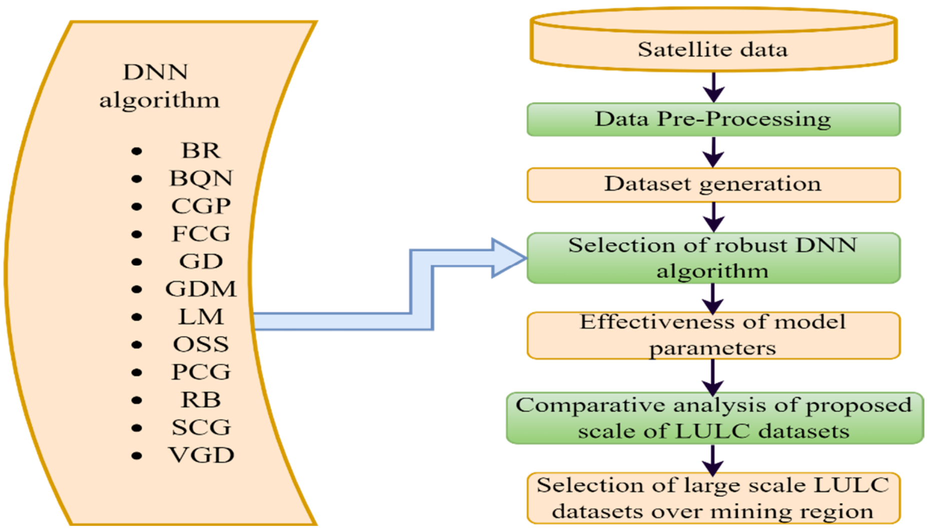

Figure 1. Flow chart of proposed method.

Table 2. Spectral bands of sentinel data used in LU classification.

Description	Band	Central wavelength (nm)	Resolution (m)
Blue	B2	490	10
Green	B3	560	10
Red	B4	665	10

2.2. Products of datasets

The database was prepared from the FCC image in three scale sizes [(1 x 1), (5 x 5), and (10 x 10)] to analyze the effect of image size on classification accuracy. In each case, the width and height of the images are considered to be the same. To generate the dataset for any individual class, the pixels in the images that represent that class were extracted from different patches. The process is repeated to obtain the desired number of images for each category, as dataset preparation of design algorithm flowchart shown in Figure 2. In the current work, a total of 5000 image samples were extracted for each of the five classes (barren land, built-up area, waterbody, vegetation, and active coal mining region). Furthermore, the datasets of three sizes were generated using a similar method for a comparative study.

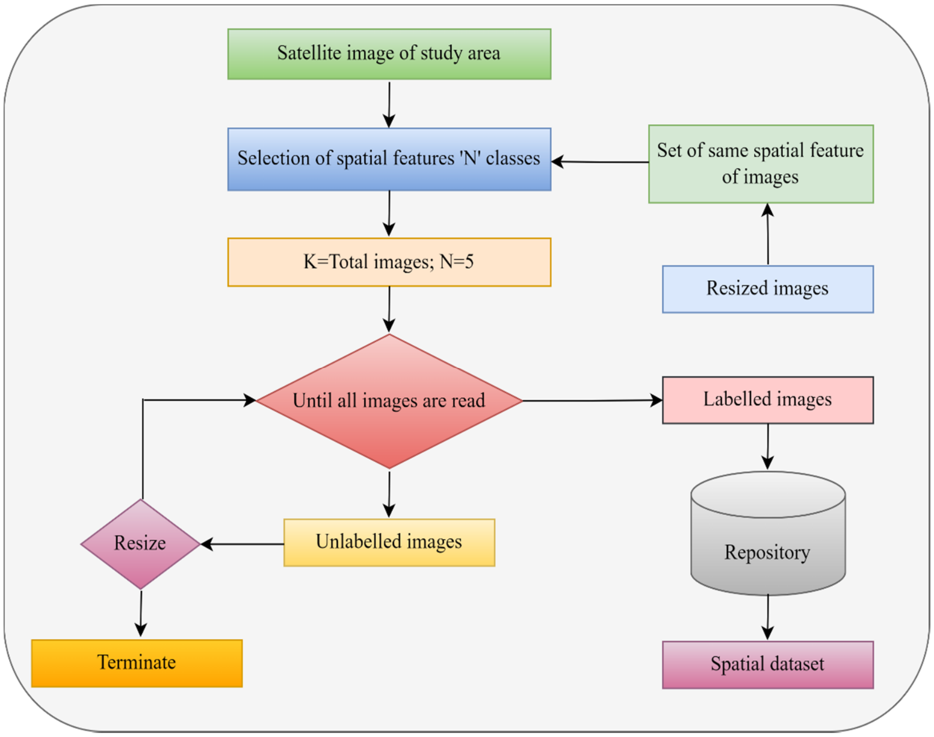

Figure 2. Proposed algorithm flowchart of LU datasets.

2.3. Model development

The conventional technique is to use the performance of the LU classification under certain conditions, such as ground control points and high-resolution scenes; also, the handling of satellite samples for the proposed DNN model using the LU classification. Deep learning is termed a universal approximator because of its mapping from input to output as y = f(x) to find out correlation among attributes x and y present in the dataset. Neural networks are modeled based on the working of the human brain for pattern recognition. DNN differs from the conventional neural network in-depth, consisting of more than one hidden layer apart from the input and output layer. Therefore, deep learning is also called a stacked neural network. A minimum of three hidden layers can be thought of as deep learning. Deep learning further can have a feature hierarchy since they combine and aggregate the features from one layer to the next. This way, it increases complexity and level of abstraction and makes it a viable choice for handling exceptionally large and high-dimensional complex datasets. Let us assume a datasets interest is the domain of defined classified regions, classified patch samples $(i = j)$ at $i, j \in 1,2,3, \dots, n$, S is total number of classifiers $AOI \to M_{i\times j}, q\epsilon S.$, Maximizing the probability of $q(g) = m_{i\times j}$, where, $m_{i\times j} \in M_{i\times j}$ are the ground truth patch samples of g, $m_{i\times j} =$ arg $max_i P((m_{i\times j})_i/g)$.

The DNN model is computing images by training, testing, and validating of different scale sizes of datasets. Also, we have used different standard training algorithms in the proposed DNN model. The examinations of twelve training algorithms are used in the DNN model. Thus, Levenberg-Marquardt (LM) is the quasi-newton methods-based approached hessian matrix used to compute performance [6]. Bayesian Regularization (BR) is the LM optimization-based approach used to the weight and bias values [15]. BFGS Quasi-Newton (BQN) is an iterative method for solving unconstrained nonlinear optimization problems [5]. Resilient Back-Propagation (RB) is a learning heuristic in feed-forward ANN [20]. Scaled Conjugate Gradient (SCG) is supervised learning with a superliner convergence rate and a member of the class of conjugate gradient methods [16]. Conjugate Gradient with Powell (CGP) is used for SCG, and the search direction will be periodically reset to the negative of the gradient [18]. Fletcher-Powell Conjugate Gradient (FCG) is updated the weights and biases according to the back-propagation gradient convergence [9]. Polak-Ribiere Conjugate Gradient (PCG) is the usage of conjugate gradient methods and is restricted to solving smooth optimization problems so far [12]. One Step Secant (OSS) is an attempt to bridge the gap between the conjugate gradient and the quasi-newton algorithm [2]. Variable Learning Rate Gradient Descent (VGD) is a very slow rate of convergence and a high dependency on the value of the learning rate parameter [3]. Gradient Descent with Momentum (GDM) is an iterative method for optimizing an objective function with suitable smoothness properties [14]. Gradient Descent (GD) is a first-order iterative optimization algorithm for finding a local minimum of a differentiable function [3] [8].

The number of epochs is neither to be very less for better parameter learning nor to be exceptionally large, to avoid overfitting on the training data. Iteration defines the number of mini-batch-wise parameter updates in a row. Mini-Batch refers to the number of examples considered at a time for computing gradients and parameter updates. Even though the choice of mini-batch size largely depends on the applications, a size of 1 will not provide the benefits of parallelism; size of 10 will be too small for GPU but acceptable for CPU; but, a size of more than 10 to 100 may provide expected results. The DNN needs many hyper-parameters to be set for implementation and at the same time; it is to be noted that finding the optimal set of values for that hyper-parameter may not be feasible using a gradient descent algorithm due to several constraints like the dataset is a mix of both real and discrete; each hyper-parameter is difficult to be optimized alone and finding local minima involves a great deal of time. Initially, the weights of a DNN are small enough so that the activation function (SoftMax activation function is used here) operates linearly with a large gradient value. The learning rate of the DNN should be chosen efficiently so that the validation error is kept to a minimum. Further, looking at the input, more network capacity is required, and hence, we are looking for many hidden layers. The L1 or L2 regularization scheme is needed to check whether the deep neural network can provide better solutions. In this process, three hidden layers are considered with the ReLU function, whereas at the output layer, SoftMax activation functions combined with multi-class cross-entropy are considered in **Figure 3.** No hidden layer should be less than a quarter of the input layer's nodes. For larger data sizes, more hidden layers are advised. At the same time, if one chose several hidden layers as same as that of input nodes, then there is a chance of identity loss and at the same time, too many hidden layers may result in noise and overfitting. To avoid overfitting, L1 and L2 regularization may be employed.

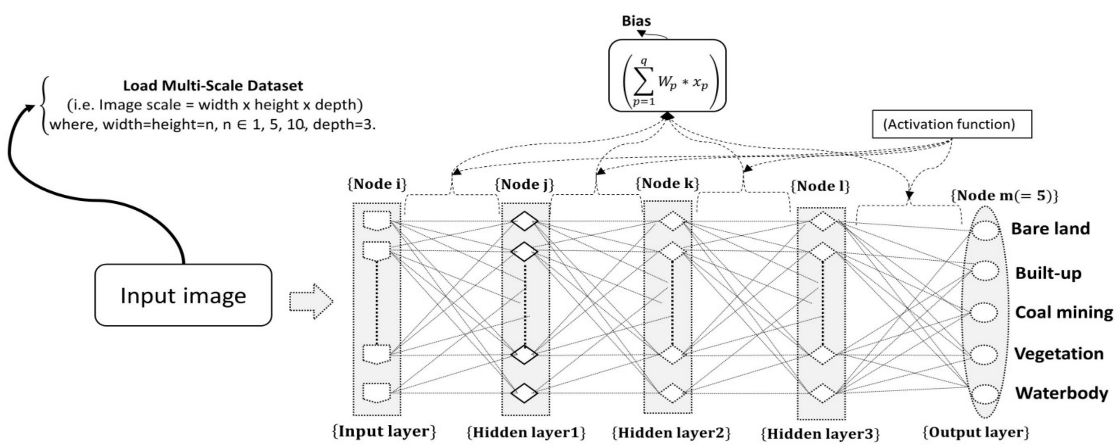

Figure 3. Architecture of DNN.

3. Evaluation of datasets on performances of different training algorithms

Image samples of satellite data were designed in three different scale sizes [(1 x 1), (5 x 5), and (10 x 10)] for examining the performances of different training algorithms. A set of 1000 image samples for each class was designed for training, testing, and validation of the model. The land surface in the selected mining region was classified into five types including barren land, built-up area, waterbody, vegetation, and active coal mine. The image datasets in three defined scale sizes [(1 × 1), (5 × 5), and (10 × 10)] representing five classes are shown in Figure 4, 5, and 6, respectively.

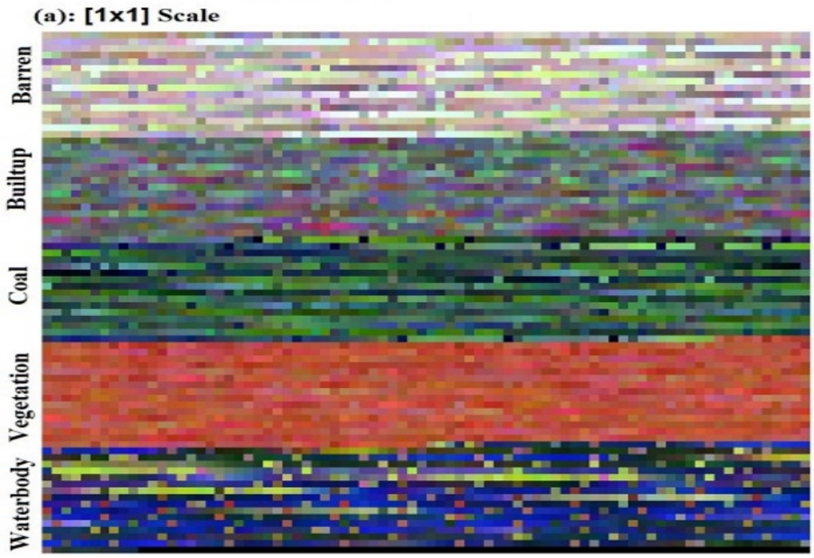

Figure 4. [1 × 1] scale sizes dataset with five class viz. barren land, built-up area, active coal mine, vegetation, and water body.

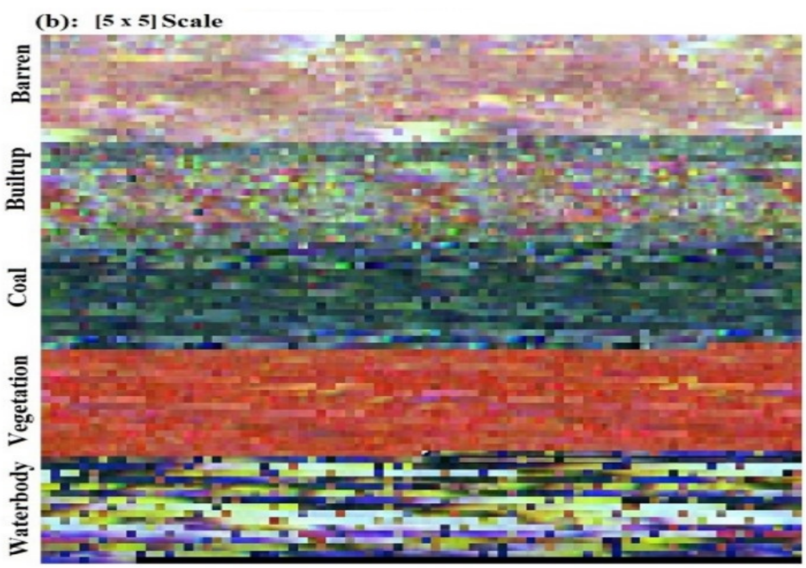

Figure 5. [5 × 5] scale sizes dataset with five class viz. barren land, built-up area, active coal mine, vegetation, and water body.

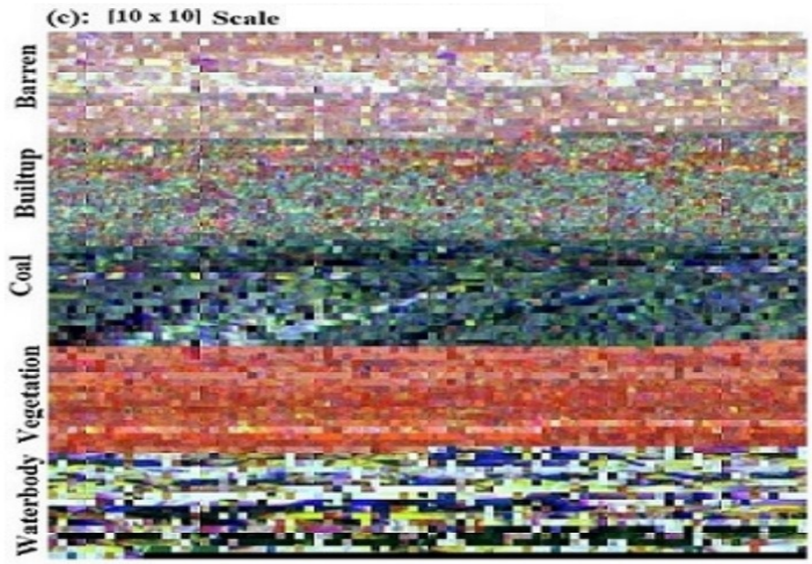

Figure 6. [10 × 10] scale sizes dataset with five class viz. barren land, built-up area, active coal mine, vegetation, and water body.

The input data layer is layout to feed sample image to the whole network. In this layer, we have found the size of sample used to train model. Size of sample is found by width, height, and number of bands for each sample of image cum number of sample images used by the DNN model. The hidden layer is designed to feed information of input layer and it is used pre-training stage of parameters. The output layer is designed to get class with the highest probability that it is used sigmoid activation function for accuracy assessment of the LU classification.

3.1. Parameter setting of DNN model

The DNN learning is followed by the feed forward network for all twelve training algorithms viz. LM, BR, BQN, RB, SCG, CGP, FCG, PCG, OSS, VGD, GDM, and GD. The parameter is chosen of common for all twelve algorithms such as listed in Table 3**.** These twelve algorithms are common outcome of results terms viz. best performance (BP), best training performance (BTP), best validation performance (BVP), gradient (G), and overall accuracy (OAA).

Table 3. Pre-training stage of parameters.

Sl. No.	Pre-training stage	Values
1	Input neuron	3, 75,300
2	Hidden1 neuron	3, 50, 221
3	Hidden 2 neuron	4, 40, 152
4	Hidden 3 neuron	4, 22, 76
5	Number of epochs	0 to 1000
6	Learning rate	0.01
7	Validation failure	0 to 6
8	Gradient	1e-5 to 1e-10
9	Activation function	sigmoid

4. Results and discussion

The results are carried out to find the impact of changing the sample image scales scale sizes [(1 × 1), (5 × 5), and (10 × 10)] on the classification performance. The experimental work is conducted by using MATLAB R2009b software and details of computer processor Intel(R) Core (TM) i5-8300H CPU @2.30 GHz, 2304Mhz, 4 core (s), 8 Logical process(s) and 8 GB RAM. The accuracy results are compared with the performance of the state-of-the-art results in these three scales of dataset listed as Tables (4, 5, 6).

Table 4. Scale sizes of (1 × 1) dataset results of DNN learning using training algorithms.

S.No.	Algorithm	No. of epochs	BP	BVP	BTP	G	OAA (%)
1	LM	20	3.06E-09	4.80E-06	7.03E-07	2.93E-08	100
2	BR	37	2.31E-09	NaN	4.25E-08	5.90E-08	100
3	BQN	74	1.87E-04	5.66E-05	3.95E-04	0.00066	100
4	RB	67	2.32E-04	0.0011	8.97E-04	0.000442	100
5	SCG	161	1.31E-07	3.47E-07	3.68E-05	9.29E-07	100
6	CGP	124	0.0446	0.0415	0.0475	8.47E-11	85.5
7	FCG	73	0.0405	0.0342	0.0396	0.000445	77.3
8	PCG	115	6.26E-12	8.40E-12	3.12E-09	4.39E-11	100
9	OSS	90	5.13E-04	6.44E-04	0.001	0.00144	100
10	VGD	278	9.80E-06	4.24E-05	8.12E-05	9.61E-06	100
11	GDM	1000	0.248	0.2865	0.2636	0.107	42
12	GD	1000	0.1077	0.1303	0.1123	0.0729	70.7

Table 5. Scale sizes of (5 × 5) dataset results of DNN learning using training algorithms.

S.No.	Algorithm	No. of epochs	BP	BVP	BTP	G	OAA (%)
1	LM	24	4.26E-06	0.028	0.0797	2.98E-08	78
2	BR	61	4.00E+00	NaN	0.055	2.78E-08	80.7
3	BQN	30	0.0576	0.067	0.0768	0.035	76
4	RB	67	0.0447	0.0601	0.0625	0.0103	72
5	SCG	40	0.0535	0.076	0.0756	0.0278	79.3
6	CGP	34	0.0472	0.0535	0.0673	0.0165	82.7
7	FCG	19	0.1801	0.196	0.1847	0.0264	33.3
8	PCG	20	0.114	0.1423	0.1384	0.0111	47.3
9	OSS	39	0.0823	0.0929	0.0889	0.0749	72
10	VGD	201	0.0394	0.0805	0.0854	0.00667	76
11	GDM	1000	0.1854	0.1875	0.184	0.0601	40.7
12	GD	1000	0.1475	0.1505	0.1512	0.0868	33.3

Table 6. Scale sizes of (10 × 10) dataset results of DNN learning using training algorithms.

S.No.	Algorithm	No. of epochs	BP	BVP	BTP	G	OAA (%)
1	LM	15	4.10E-03	1.03E-01	1.14E-01	1.68E-07	72.7
2	BR	46	1.43E-09	NaN	9.12E-02	7.99E-08	71.3
3	BQN	46	3.49E-02	6.06E-02	8.56E-02	0.022	79.3
4	RB	34	4.94E-02	0.0786	9.32E-02	0.0145	73.3
5	SCG	52	7.51E-02	1.00E-01	9.38E-02	5.77E-02	72
6	CGP	30	0.0553	0.0698	0.0766	3.65E-02	74
7	FCG	36	0.1121	0.1319	0.1561	0.0475	51.3
8	PCG	22	6.56E-02	6.33E-02	7.80E-02	3.87E-02	68.7
9	OSS	53	7.76E-02	9.23E-02	0.1293	0.0407	55.3
10	VGD	164	3.94E-02	6.37E-02	7.48E-02	4.19E-02	71.3
11	GDM	1000	0.1407	0.1592	0.145954.7	0.0474	42.7
12	GD	1000	0.1162	0.118	0.12	0.0717	54.7

4.1. Comparison of different scale sizes of datasets

We have compared datasets for the same satellite image with different scale of sample image classes. The performance of results is varying due to changes of scale in dataset. Also, the performance of results viz. BP, BVP, BTP, G, and OAA, as shown in Figure 7. The BP, BVP, BTP, G results are [(1 × 1), (5 × 5), and (10 × 10)] scale sizes of dataset in the GDM training algorithm best result among all scale of dataset Figure 8. However, the overall accuracy results are [(1 × 1), (5 × 5), and (10 × 10)] scale sizes of dataset in the VGD, OSS, PCG, SCG, RB, BQN, BR, and LM training algorithm 90% to approximate 100 % result among all scale of dataset.

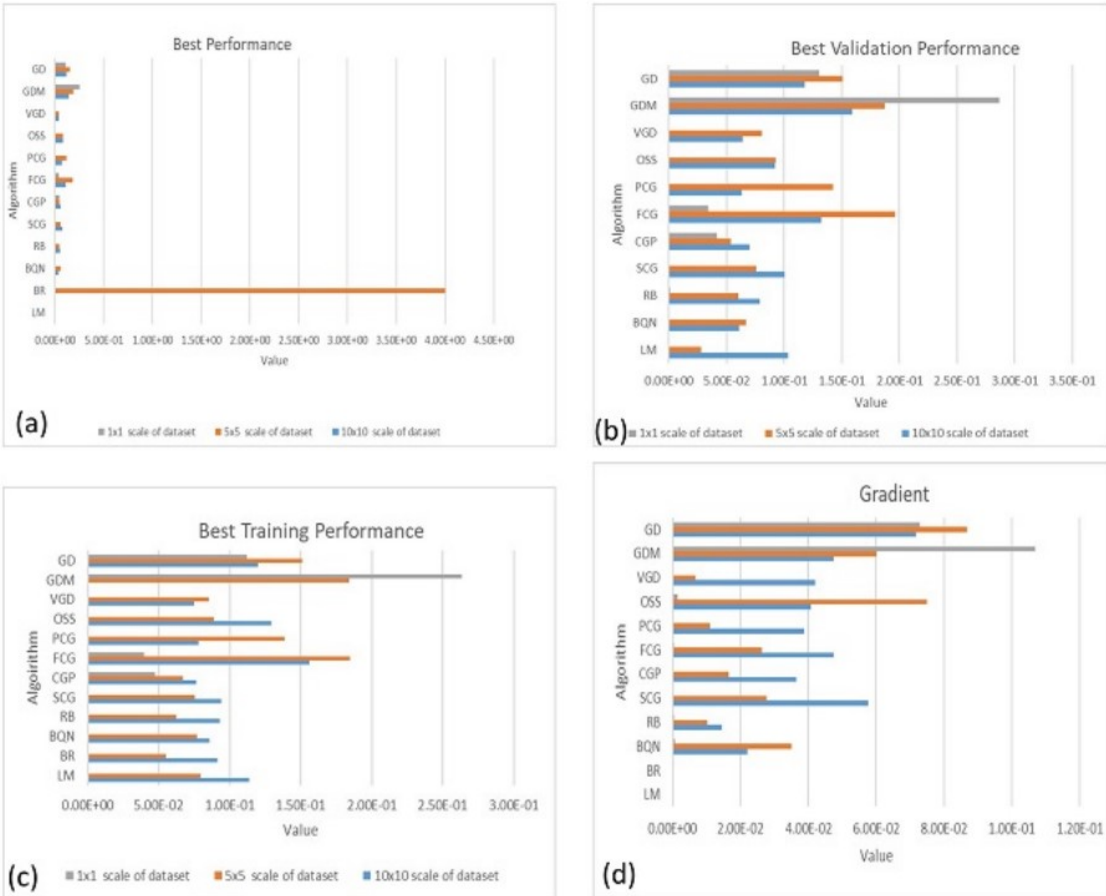

Figure 7. Different training algorithm-based performances change in [(1 × 1), (5 × 5), and (10 × 10)] scale sizes of datasets.

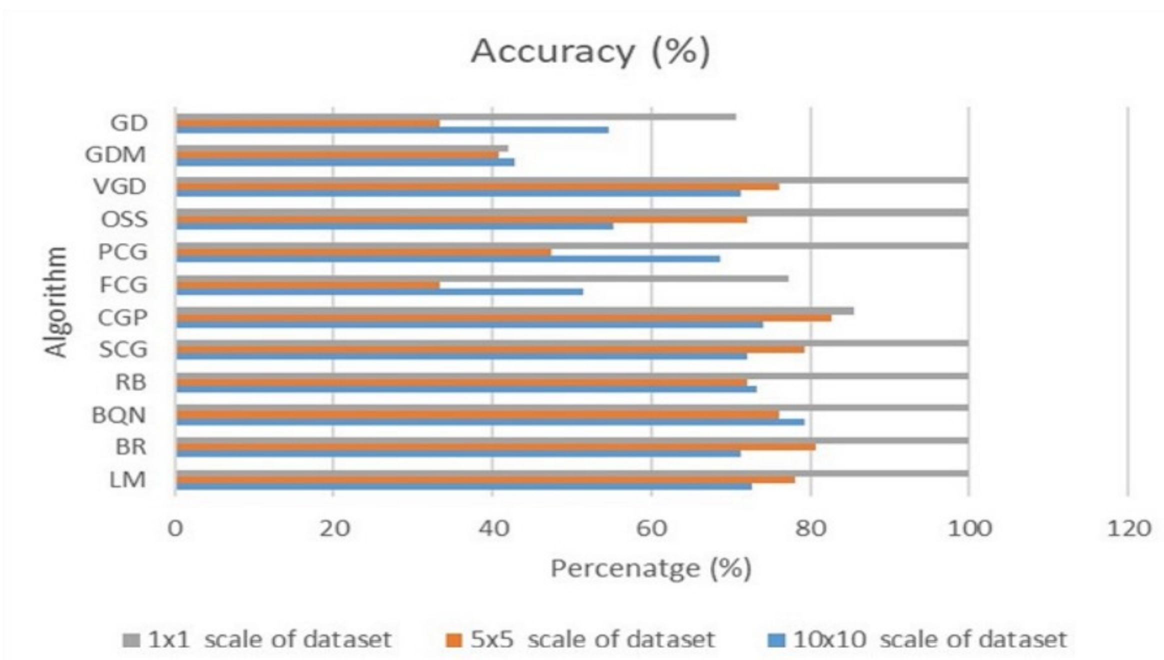

Figure 8. Different training algorithm-based accuracy changes in [(1 × 1), (5 × 5), and (10 × 10)] scale sizes of datasets.

5. Conclusions

Scale sizes of dataset generation in satellite image processing is an important and challenging step for remote sensing applications, especially the LU classification. In present study, we generated a dataset of an adequate scale size to be used in DNN learning for the LU classification over mining activities region, which is much more specialized and suitable than other general datasets. The adopted DNN learning performances have higher accuracy in (1 × 1) scale of dataset. From the experiments, it is observed that performance of proposed approach increases with a scale size from (10 × 10), (5 × 5) and (1 × 1) of datasets. Apart from this, our proposed approach is very convenient for processing large-scale satellite image dataset using the LU classification. In the future, advanced learning techniques will be introduced for fast computing and achieving higher accuracy levels.

Conflict of Interest:

There is no conflict of interests involved.

Funding:

Not applicable.

Abbreviations

LM	Levenberg-Marqardt
BR	Bayesian Regularization
BQN	BFGS Quasi-Newton
RB	Resilient Back Propagation
OSS	One Step Secant
VGD	Variable Learning Rate Gradient Descent
SEG	**Scaled Conjugate Gradient**
CGP	Conjugate Gradient with Powell
FCG	Fletcher-Powell Conjugate Gradient
PCG	Polak-Ribiere Conjugate Gradient
GDM	Gradient Descent with Momentum
GD	Gradient Descent

References

[1]. Balha, A., Mallick, J., Pandey, S., Gupta, S., and Singh, C.K. (2021). A comparative analysis of different pixel and object-based classification algorithms using multi-source high spatial resolution satellite data for LULC mapping. Earth Science Informatics, 14 (4): 2231-2247.

[2]. Battiti, R. (1992). First-and second-order methods for learning: between steepest descent and Newton's method. Neural computation, 4 (2): 141-166.

[3]. Bottou, L. (2003). Stochastic learning. In Summer School on Machine Learning (pp. 146-168). Springer, Berlin, Heidelberg.

[4]. Castelluccio, M., Poggi, G., Sansone, C., and Verdoliva, L. (2015). Land use classification in remote sensing images by convolutional neural networks. arXiv preprint arXiv:1508.00092.

[5]. Gill, P.E., Murray, W., and Wright, M.H. (2019). Practical optimization. Society for Industrial and Applied Mathematics.

[6]. Hagan, M.T., and Menhaj, M.B. (1994). Training feedforward networks with the Marquardt algorithm. IEEE transactions on Neural Networks, 5(6): 989-993.

[7]. Hay, G. J., and Castilla, G. (2008). Geographic Object-Based Image Analysis (GEOBIA): A new name for a new discipline. In Object-based image analysis (pp. 75-89). Springer, Berlin, Heidelberg.

[8]. Jin, C., Netrapalli, P., and Jordan, M.I. (2018). Accelerated gradient descent escapes saddle points faster than gradient descent. In Conference On Learning Theory (pp. 1042-1085). PMLR.

[9]. Johnson, R.A., and Wichern, D.W. (2020). Applied multivariate statistical analysis.

[10]. Kumar, A., and Gorai, A.K. (2022). Application of transfer learning of deep CNN model for classification of time-series satellite images to assess the long-term impacts of coal mining activities on land-use patterns. Geocarto International, 1-21.

[11]. Laban, N., Abdellatif, B., Ebied, H. M., Shedeed, H.A., and Tolba, M.F. (2017). Performance enhancement of satellite image classification using a convolutional neural network. In International Conference on Advanced Intelligent Systems and Informatics (pp. 673-682). Springer, Cham.

[12]. Labat, C., and Idier, J. (2006). Preconditioned conjugate gradient without linesearch: a comparison with the half-quadratic approach for edge-preserving image restoration. In Computational Imaging IV (Vol. 6065, pp. 134-143). SPIE.

[13]. Lee, H., and Kwon, H. (2016). Contextual deep CNN based hyperspectral classification. In 2016 IEEE international geoscience and remote sensing symposium (IGARSS) (pp. 3322-3325). IEEE.

[14]. Lemaréchal, C. (2012). Cauchy and the gradient method. Doc Math Extra, 251(254). 10.

[15]. MacKay, D.J. (1992). Bayesian interpolation. Neural computation, 4(3): 415-447.

[16]. Møller, M.F. (1990). A scaled conjugate gradient algorithm for fast supervised learning. Aarhus University. Computer Science Department, 339.

[17]. Pesaresi, M., Huadong, G., Blaes, X., Ehrlich, D.,

Ferri, S., Gueguen, L., and Zanchetta, L. (2013). A global human settlement layer from optical HR/VHR RS data: Concept and first results. IEEE Journal of Selected Topics in Applied Earth Observations and Remote Sensing, 6(5): 2102-2131.

[18]. Powell, M.J.D. (1977). Restart procedures for the conjugate gradient method. Mathematical programming, 12(1): 241-254.

[19]. Qu, L. A., Chen, Z., Li, M., Zhi, J., and Wang, H. (2021). Accuracy improvements to pixel-based and object-based lulc classification with auxiliary datasets from Google Earth engine. Remote Sensing, 13(3): 453.

[20]. Riedmiller, M., and Braun, H. (1993). A direct adaptive method for faster backpropagation learning: the RPROP algorithm. In IEEE international conference on neural networks (pp. 586-591).

[21]. Simon, C., and De Vleeschouwer, C. (2021). Intraclass clustering: an implicit learning ability that regularizes DNNs. arXiv preprint arXiv:2103.06733.

[22]. Trujillo-Jiménez, M.A., Liberoff, A.L., Pessacg, N., Pacheco, C., Díaz, L., and Flaherty, S. (2022). SatRed: New classification land use/land cover model based on multi-spectral satellite images and neural networks applied to a semiarid valley of Patagonia. Remote Sensing Applications: Society and Environment, 26, 100703.

[23]. Verma, D., and Jana, A. (2019). LULC classification methodology based on simple Convolutional Neural Network to map complex urban forms at finer scale: Evidence from Mumbai. arXiv preprint arXiv:1909.09774.

[24]. Xia, G. S., Hu, J., Hu, F., Shi, B., Bai, X., Zhong, Y., and Lu, X. (2017). AID: A benchmark data set for performance evaluation of aerial scene classification. IEEE Transactions on Geoscience and Remote Sensing, 55(7): 3965-3981.

[25]. Xia, G.S., Yang, W., Delon, J., Gousseau, Y., Sun, H., and Maître, H. (2010). Structural high-resolution satellite image indexing. In ISPRS TC VII Symposium-100 Years ISPRS,Vol. 38, pp. 298-303.

[26]. Zhang, C., Sargent, I., Pan, X., Li, H., Gardiner, A., Hare, J., and Atkinson, P.M. (2018). An object-based convolutional neural network (OCNN) for urban land use classification. Remote sensing of environment, 216, 57-70.

یک شبکه عصبی عمیق برای طبقه‌بندی مجموعه داده‌های ماهواره‌ای کاربری زمین در محیط‌های معدنی

آجی کومار، یادوندرا پراتاپ سینگ، آدیتیا گوپتا*، و مونو باگات

دانشکده علوم کامپیوتر و فناوری اطلاعات، دانشگاه مانیپال جیپور، جیپور، راجستان، هند

ارسال ۲۰۲۲/۰۹/۰۸، پذیرش ۲۰۲۲/۰۹/۲۷

*نویسنده مسئول مکاتبات:aditya.gupta@jaipur.manipal.edu

چکیده:

کاربری زمین (LU) یکی از ضروری‌ترین بخش‌های اطلاعات نقشه برداری است که برای نظارت بر محیط معدن استفاده می‌شود. استخراج مجموعه داده‌های کاربری زمین از تصاویر ماهواره‌ای سنجش از راه دور، توجه قابل توجهی را در جامعه منطقه معدنی به خود جلب کرده است. با این حال، طبقه‌بندی LUs از تصاویر ماهواره‌ای به دلیل در دسترس نبودن مجموعه داده‌های مرتبط با استخراج زغالسنگ کارآمد، یک کار خسته‌کننده است. روش‌های یادگیری عمیق اهرم بزرگی برای استخراج اطلاعات معنی‌دار از تصاویر ماهواره‌ای با وضوح بالا فراهم می‌کند. علاوه بر این، عملکرد یک رویکرد طبقه بندی یادگیری عمیق به طور قابل توجهی به کیفیت مجموعه داده‌ها بستگی دارد. کار حاضر تلاش می‌کند تا تولید مجموعه‌های داده مبتنی بر ماهواره را برای تحلیل عملکرد الگوریتم‌های یادگیری مبتنی بر شبکه‌های عصبی عمیق (DNN) در طبقه‌بندی‌های LU مناطق معدنی نشان دهد. مناطق معدن به طور کلی بر اساس بازرسی بصری به مناطق مجزایی زمین‌های بایر، مناطق ساخت و ساز شده، بدنه آبی، پوشش گیاهی و معادن زغالسنگ فعال طبقه بندی می‌شوند. در کار تجربی ما، یک روش و راه از ۱۰۰ نمونه فضایی برای هر یک از پنج ویژگی در سه مقیاس، به‌عنوان [۱×۱×۳]، [۵×۵×۳] و [۱۰×۱۰×۳] تولید می‌شود. علاوه بر این، اثرات مقیاس پذیری‌های مختلف مجموعه داده بر عملکرد طبقه بندی نیز تجزیه و تحلیل می‌شود. همچنین این مطالعه موردی برای معیار مقیاس بزرگ مجموعه داده‌های تصاویر ماهواره‌ای برای مناطق معدنی اجرا شده است. در آینده، این کار می‌تواند برای طبقه بندی LU در مناطق مورد مطالعه مربوطه در زمان واقعی استفاده شود.

کلمات کلیدی: تصویر ماهواره ای، مجموعه داده، منطقه معدن، کاربری زمین، شبکه عصبی عمیق.